Dalton Transactions

Accepted Manuscript

ROYAL SOCIETY OF CHEMISTRY

www.rsc.org/dalton

Kinetics of cisplatin binding to short r(GG) containing miRNA mimics – influence of Na^+ *versus* K^+, temperature and hydrophobicity on reactivity

Alak Alshiekh,[a] Maria Clausén[a] and Sofi K.C. Elmroth[a]

Figure Captions

Figure 1. (A) Spectra as a function of time after addition of **1a** to RNA-1-3-X in Buffer A (C_{Na+} = 122 mM), collected every 25 min in the time interval 0 - 225 min after mixing. (B) Representative kinetic traces after addition of **1a** to RNA-1-1 (dark green), RNA-1-1-S (light green), and RNA-1-3-X (dark blue); $C_{\mathbf{1a}}$ = 15 µM, C_T = 3.0 µM, T = 38 $_o$C, C_{K+} = 122 mM (Buffer B), together with exponential fits (black). (C) Representative kinetic trace after addition of **1a** to RNA-1-3 (light blue); $C_{\mathbf{1a}}$ = 15 µM, C_T = 3.0 µM, T = 28 $_o$C, C_{K+} = 122 mM (Buffer B), together with exponential fits (black).

Figure 2. (A) and (B) Absorbance change as a function of time (gray), together with fits of a single-exponential function to experimental data (solid lines), after addition of **1a** to RNA-1-3-X. Measurements were conducted with $C_{\mathbf{1a}}$ = 7.5 - 45.0 µM, C_T = 3.0 µM and T = 38 °C in buffered solution, (A) C_{Na+} = 122 mM (Buffer A). (B) C_{K+} = 122 mM (Buffer B). (C) Observed pseudo-first-order rate constants (k_{obs}) for reaction with RNA-1-3-X, and plotted as a function of $C_{\mathbf{1a}}$ in the interval 7.5 - 45.0 µM together with linear regression lines, allowing for determination of $k_{2,app}$ from the slope. All measurements were conducted in triplicates with C_T = 3.0 µM. Experimental data points obtained at C_{Na+} = 122 mM are shown as triangles, and data points at C_{K+} = 122 mM as squares, with corresponding linear regression lines in blue and purple, respectively.

Figure 3. Absorbance change as a function of temperature and time, and corresponding Eyring plot. (A) RNA-1-1-S melting curve, the arrows indicate the temperatures used for the temperature dependence study. (B) Absorbance change as a function of time after addition of **1a** to RNA-1-1-S followed at λ = 260 nm; T = 33, 38, 43, and 48 °C (blue, green, pink and red). All measurements were conducted with $C_{\mathbf{1a}}$ = 45.0 µM, C_T = 3.0 µM in Buffer B. (C) Eyring plot of the reaction of **1a** with RNA-1-1-S with linear regression allowing for determination of $\Delta H^{\ddagger}$ and $\Delta S^{\ddagger}$.

Figure 4. Comparison of modelled structures for side- and top views, together with a schematic representation of the hydrogen bonding patterns with minimized distances (noted in Å) around the four central base pairs of (A) r(UGGU).r(ACCA) in RNA-1-1, and (B) r(UGGU).r(AUAUA) in RNA-1-3.

Table 1. Summary of melting temperatures and apparent second-order rate constants obtained at 38 ºC for reactions of **1a** with RNA-1-1, RNA-1-1-S, RNA-1-3-X, and RNA-1-3.

Duplex	C_{Na+} = 122 mM		C_{K+} = 122 mM		C_{Na+} = 50 mM		C_{Na+} = 50 mM and 10% EtOH	
	T_m (ºC)	$k_{2,app}$ ($M^{-1}s^{-1}$)	T_m (ºC)	$k_{2,app}$ ($M^{-1}s^{-1}$)	T_m (ºC)	$k_{2,app}$ ($M^{-1}s^{-1}$)	T_m (ºC)	$k_{2,app}$ ($M^{-1}s^{-1}$)
RNA-1-1	61.6 ± 0.2	7.7±0.5[a]	59.5±0.3	9.2±0.6	54.9±0.1	21±5	53.7±0.5	12.9±1.4
RNA-1-1-S	56.7 ± 0.1	10.5±0.6[a]	55.0±0.2	12.6±1.1	49.8±0.1	26.1±0.2	46.7±0.8	16±2.5
RNA-1-3-X	53.1 ± 0.2	15.8±0.3	50.9±0.1	19.4±1.2	47.3±0.3	39±5	46.3±0.1	24.3±1.5
RNA-1-3	39.2 ± 0.1	29.7±1.1[a]	36.5±0.3	*n.d.*	32.5±0.2	*n.d.*	33.0±0.2	*n.d.*
RNA-1-3	39.2 ± 0.1	6.0±0.5[b]	36.5±0.3	8.0±0.6[b]	32.5±0.2	15.7±1.8[b]	33.0±0.2	10.7±0.5[b]

[a] Data from Ref# 3n, [b] $k_{2,app}$ determined at 28 ºC.

RNA-1-1-S	(a)	5´-UU CUU GGU UCU CU-3´
	(b)	3´-AA GAA CCA AGA GA-5´
RNA-1-1	(a)	5´-CUU CUU GGU UCU CUU-3´
	(b)	3´-GAA GAA CCA AGA GAA-5´
RNA-1-3	(a)	5´-CUU CUU G GU UCU CUU-3´
	(b)	3´-GAA GAA UAUA AGA GAA-5´
RNA-1-3-X	(a)	5´-CUU CUU CUU G GU UCU CUU CU-3´
	(b)	3´-GAA GAA GAA UAUA AGA GAA GA-5´

Scheme 1. Schematic illustration of used RNA sequences and metal reagent.

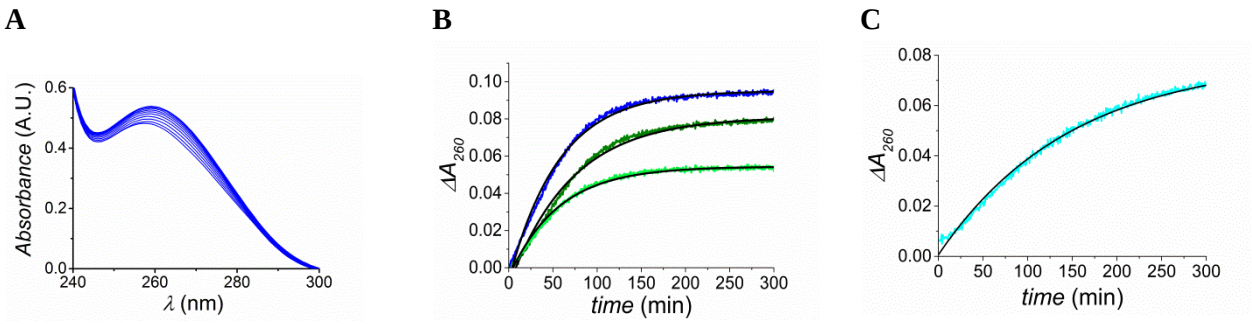

Figure 1. (A) Spectra as a function of time after addition of **1a** to RNA-1-3-X in Buffer A (C_{Na+} = 122 mM), collected every 25 min in the time interval 0 - 225 min after mixing. (B) Representative kinetic traces after addition of **1a** to RNA-1-1 (dark green), RNA-1-1-S (light green), and RNA-1-3-X (dark blue); $C_{\mathbf{1a}}$ = 15 µM, C_T = 3.0 µM, T = 38 °C, C_{K+} = 122 mM (Buffer B), together with exponential fits (black). (C) Representative kinetic trace after addition of **1a** to RNA-1-3 (light blue); $C_{\mathbf{1a}}$ = 15 µM, C_T = 3.0 µM, T = 28 °C, C_{K+} = 122 mM (Buffer B), together with exponential fits (black).

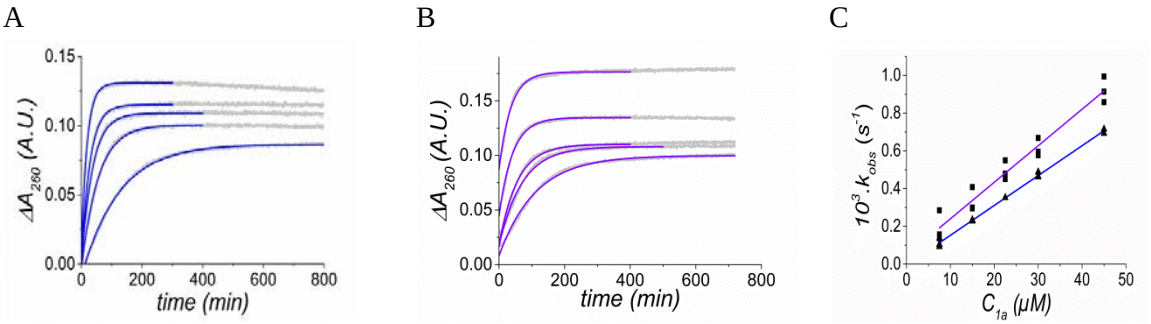

Figure 2. (A) and (B) Absorbance change as a function of time (gray), together with fits of a single-exponential function to experimental data (solid lines), after addition of **1a** to RNA-1-3-X. Measurements were conducted with $C_{\mathbf{1a}}$ = 7.5 - 45.0 μM, C_T = 3.0 μM and T = 38 °C in buffered solution, (A) C_{Na+} = 122 mM (Buffer A). (B) C_{K+} = 122 mM (Buffer B). (C) Observed pseudo-first-order rate constants (k_{obs}) for reaction with RNA-1-3-X, and plotted as a function of $C_{\mathbf{1a}}$ in the interval 7.5 - 45.0 μM together with linear regression lines, allowing for determination of $k_{2,app}$ from the slope. All measurements were conducted in triplicates with C_T = 3.0 μM. Experimental data points obtained at C_{Na+} = 122 mM are shown as triangles, and data points at C_{K+} = 122 mM as squares, with corresponding linear regression lines in blue and purple, respectively.

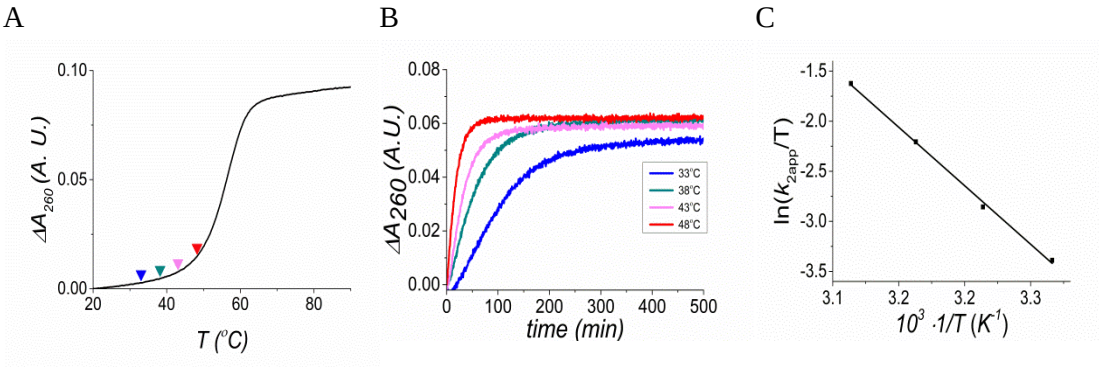

Figure 3. Absorbance change as a function of temperature and time, and corresponding Eyring plot. (A) RNA-1-1-S melting curve, the arrows indicate the temperatures used for the temperature dependence study. (B) Absorbance change as a function of time after addition of **1a** to RNA-1-1-S followed at λ = 260 nm; T = 33, 38, 43, and 48 °C (blue, green, pink and red). All measurements were conducted with $C_{\mathbf{1a}}$ = 45.0 μM, C_T = 3.0 μM in Buffer B. (C) Eyring plot of the reaction of **1a** with RNA-1-1-S with linear regression allowing for determination of $\Delta H^{\neq}$ and $\Delta S^{\neq}$.

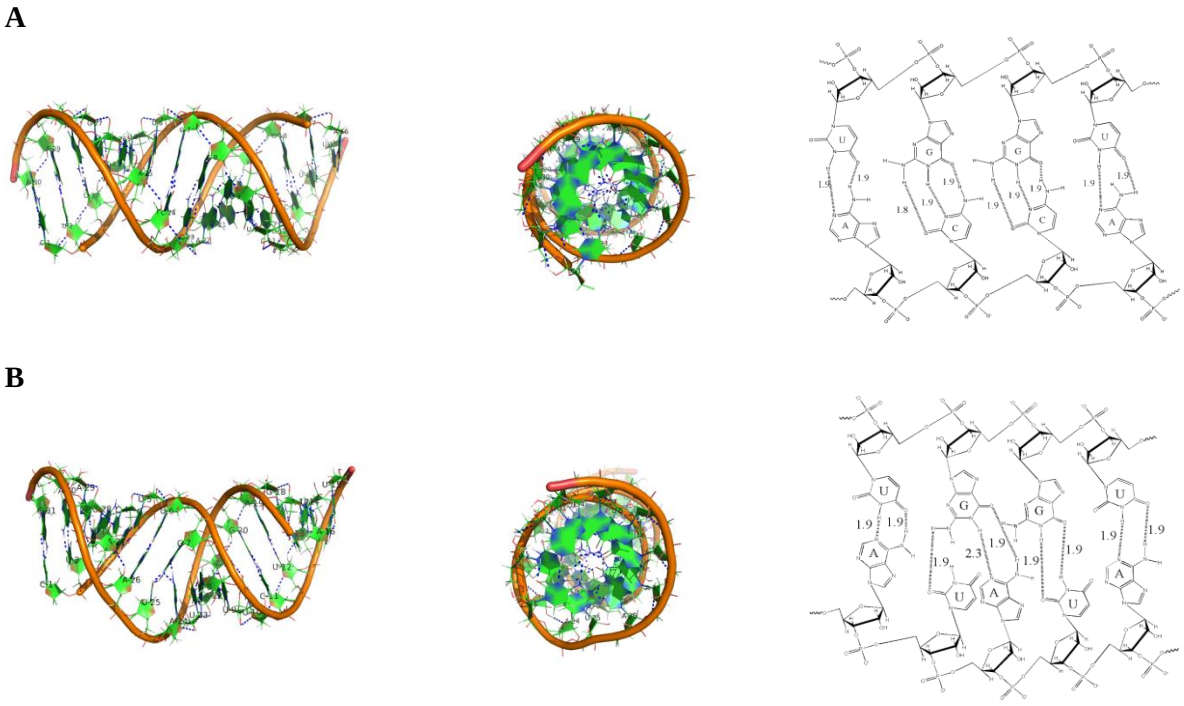

Figure 4. Comparison of modelled structures for side- and top views, together with a schematic representation of the hydrogen bonding patterns with minimized distances (noted in Å) around the four central base pairs of (A) r(UGGU)·r(ACCA) in RNA-1-1, and (B) r(UGGU)·r(AUAUA) in RNA-1-3.

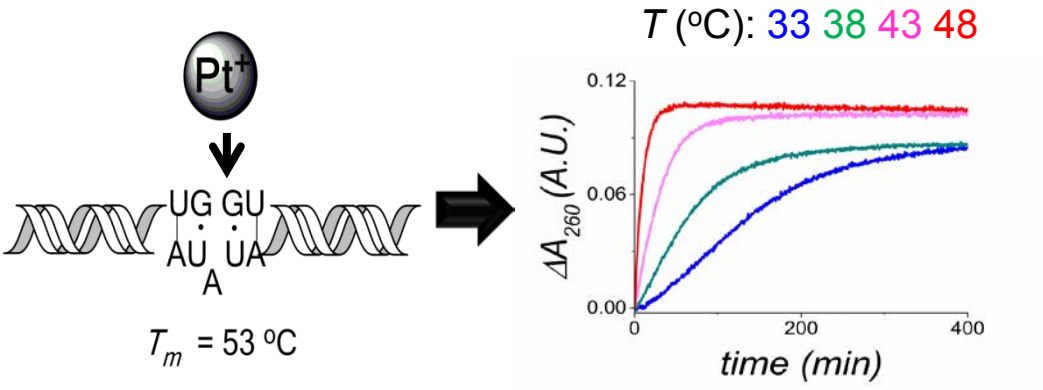

Table 2. Comparison of experimentally determined rate constants and activation parameters for dsRNAs and related model systems with reactions between Pt-based metal complexes and G-N7 containing nucleophiles, together with calculated thermodynamic parameters for melting of the dsRNAs at C_{Na+}= 1.0 M.

Reaction	T_m (°C)	Rate constant and activation parameters for platination	Thermodynamic parameters for duplex melting at C_{Na+}= 1.0 M[c]
RNA-1-3 + **1a**[a] T = 38 °C C_{Na+} = 122 mM, pH 5.8	39.2	$k_{2,app}$ = 29.7 ± 1.1 $M^{-1}s^{-1}$ $\Delta H^{\neq}$ = 29 ± 4 $kcalmol^{-1}$ $\Delta S^{\neq}$ = 42 ± 7 $calK^{-1}mol^{-1}$	ΔG^o = 18.8 $kcalmol^{-1}$ ΔH^o = 122 $kcalmol^{-1}$ ΔS^o = 380 $kcalmol^{-1}$ T_m = 49.0
RNA-1-3-X + **1a**[a] T = 38 °C C_{Na+} = 122 mM, pH 5.8	53.1	$k_{2,app}$ = 15.9 ± 0.67 $M^{-1}s^{-1}$ $\Delta H^{\neq}$ = 34 ± 3 $kcalmol^{-1}$ $\Delta S^{\neq}$ = 57 ± 5 $calK^{-1}mol^{-1}$	ΔG^o = 33.6 $kcalmol^{-1}$ ΔH^o = 178 $kcalmol^{-1}$ ΔS^o = 530 $kcalmol^{-1}$ T_m = 64.1
RNA-1-1-S + **1a**[a] T = 38 °C C_{Na+} = 122 mM, pH 5.8	56.7	$k_{2,app}$ = 10.5 ± 0.6 $M^{-1}s^{-1}$ $\Delta H^{\neq}$ = 25 ± 6 $kcalmol^{-1}$ $\Delta S^{\neq}$ = 28 ± 7 $calK^{-1}mol^{-1}$	ΔG^o = 24.2 $kcalmol^{-1}$ ΔH^o = 124 $kcalmol^{-1}$ ΔS^o = 366 $kcalmol^{-1}$ T_m = 64.2
RNA-1-1 + **1a**[a] T = 38 °C C_{Na+} = 122 mM, pH 5.8	61.6	$k_{2,app}$ = 7.72 ± 0.45 $M^{-1}s^{-1}$ $\Delta H^{\neq}$ = 29 ± 4 $kcalmol^{-1}$ $\Delta S^{\neq}$ = 39 ± 5 $calK^{-1}mol^{-1}$	ΔG^o = 27.8 $kcalmol^{-1}$ ΔH^o = 137 $kcalmol^{-1}$ ΔS^o = 403 $kcalmol^{-1}$ T_m = 69.3
$Pt(dach)(OH_2)_2^{2+}$ + 5′-GMP[b] T = 40 °C I= 0.01 M HOTf, pH 2	-	k_1 = 5.8 ± 0.2 $M^{-1}s^{-1}$ $\Delta H_1^{\neq}$ = 16.7 ± 0.3 $kcalmol^{-1}$ $\Delta S_1^{\neq}$ = -1.7 ± 0.7 $calK^{-1}mol^{-1}$	-
$Pt(en)(OH_2)_2^{2+}$ + 5′-GMP[b] T = 40 °C I= 0.01 M HOTf, pH 2	-	k_1 = 3.9 ± 0.1 $M^{-1}s^{-1}$ $\Delta H_1^{\neq}$ = 15 ± 0.7 $kcalmol^{-1}$ $\Delta S_1^{\neq}$ = -7.6 ± 2.6 $calK^{-1}mol^{-1}$	-

[a] This work; C_{Na+} = 122 mM (Buffer A/B), [b] Data from Ref #33; k_1 determined at 40 °C, pH = 2 and I = 0.01 M, [c] Calculated data by use of the software provided by Ref #13.

Journal Name

RSCPublishing

ARTICLE

Kinetics of cisplatin binding to short r(GG) containing miRNA mimics – influence of Na^+ *versus* K^+, temperature and hydrophobicity on reactivity

Alak Alshiekh,[a] Maria Clausén[a] and Sofi K.C. Elmroth[a]

Cite this: DOI: 10.1039/x0xx00000x

Received 00th February 2015,
Accepted 00th February 2015

DOI: 10.1039/x0xx00000x

www.rsc.org/

Nucleic acids are well recognized targets for platinum-based anticancer drugs, with RNA and DNA being kinetically comparable. In the case of RNA, previous studies have shown that the reaction between small duplex RNAs (dsRNAs) and monoaquated cisplatin (*cis*-$Pt(NH_3)_2Cl(OH_2)^+$, **1a**) can be followed by the metal induced hyperchromicity occurring directly after addition of **1a** to *e.g.* microRNA mimics. In the present study, we have used this approach to compare thermal stability and reactivity between intracellularly- and extracellularly relevant salt concentration (C_{Na+} and C_{K+} ca. 0.1 M), and also as a function of increased hydrophobicity (10% v/v EtOH). In addition, reactivity was studied as a function of temperature in the interval ca. 5 - 20 °C below the respective dsRNA melting temperatures (T_ms). Four different 13- to 20-mer dsRNAs with two different central sequence motifs were used as targets containing either a central r(GG)·r(CC)- or r(GG)·r(UAU)-sequence. The reactions exhibited half-lives in the minute- to hour range at 38 °C in the presence of excess **1a** in the μM range. Further, a linear dependence was found between $C_{\mathbf{1a}}$ and the observed pseudo-first-order rate constants. The resulting apparent second-order rate constants were significantly larger for the lower melting r(GG)·r(UAU)-containing sequences compared with that of the fully complementary ones; the higher and lower reactivities represented by RNA-1-3 and RNA-1-1 with $k_{2,app}$ ca. 30 and 8 $M^{-1}s^{-1}$ respectively at C_{Na+} = 122 mM. For all RNAs a common small, but significant, trend was observed with increased reactivity in the presence of K^+ compared with Na^+, and decreased reactivity in the presence of EtOH. Finally, the temperature dependence of $k_{2,app}$ was evaluated using the Eyring equation. The retrieved activation parameters reveal positive values for both $\Delta H^{\neq}$ and $\Delta S^{\neq}$ for all dsRNAs, in the range ca. 23 – 34 $kcalmol^{-1}$ and 22 – 57 $calK^{-1}mol^{-1}$ respectively. These values indicate solvational effects to be important for the rate determining step of the reaction, and thus in support of a structural change of the dsRNA to take place in parallel with the adduct formation step.

Introduction

The successful clinical use of cisplatin (*cis*-$Pt(NH_3)_2Cl_2$, **1**) as an antineoplastic illustrates the capacity of platinum-based coordination compounds to interfere with malignant biological processes.[1] Here, disruption of DNA function has been well documented as a mode of action, and with induction of both apoptosis and necrosis as down-stream cellular responses.[1c] The ability of cisplatin to interact is neither exclusive to DNA nor an absolute requirement for induction of apoptosis,[2] however. Rather, facile interaction with *e.g.* RNA has been shown to occur in cellular systems and *in vitro*, although details in terms of biological response still remain to be investigated.[3]

From an accessibility point of view, RNAs are readily available for reaction with cisplatin in both the extra- and intracellular environment.[4] In order to interfere with biological function however, the rate of adduct formation has to compete with biological excretion. Further, the adducts formed should cause structural and/or functional changes of their targets that affect the cellular machinery.[5] Observations supporting RNA as a kinetically competitive target include studies by both other groups and our own, which together give an overall picture of RNA being at least as reactive as DNA.[3c, 3l, 3n, 6] In contrast to DNA however, where binding to the d(GpG) sequence is known to be strongly preferred, [1c, 1d, 7] the adduct profile patterns in RNA exhibit a more pronounced variation with local

sequence.[3c, 3e-g, 3i, 3m] These observations indicate that under *in vivo* conditions, kinetic binding preference for a common reactive target nucleobase varies significantly, and is better regarded as an effect of local structure rather than sequence alone.

The molecular RNA landscape offers a multitude of both two- and three dimensional structures. For a common binding site, it can thus be expected that the nature of surrounding sequences – as well as their response to solvent conditions – will have a strong influence on binding kinetics and resulting adduct profile. For example, adduct formation rates in the extracellular environment with high sodium ion (Na^+) concentration may be different from that in the intracellular environment where potassium ions (K^+) predominate. Further, the commonly observed co-localization of RNAs with proteins may protect from metalation by combined effects from sterics and increased hydrophobicity. To better understand how the RNA machinery responds to drug exposure, we have recently initiated studies aiming at highly accurate documentation of RNA reaction kinetics when exposed to commonly used metal-based anticancer drugs such as cisplatin. The methodology takes advantage of the hyperchromicity induced at λ = 260 nm following exposure of double-stranded RNA (dsRNA) to the intracellularly active metabolite of cisplatin (*cis*-$Pt(NH_3)_2Cl(OH_2)^+$, **1a**), see **Scheme 1**. In previous studies,[3l, 3n] we have shown that such exposure gives rise to highly reproducible kinetic data. Further, the rate constants exhibited first-order dependence on the concentration of **1a** both at low Na^+ conditions (ca. 20 mM) and at physiologically relevant extracellular conditions (ca. 0.1 M). In the present investigation, our intent has been to compare reactivities of an extended series of r(GG)-containing 13 to 20-mer duplexes, see **Scheme 1**, in the commonly used Na^+-environment with that of a system mimicking the intracellular conditions with ca. 0.1 M K^+concentration. The influence of increased hydrophobicity was also investigated by addition of 10% ethanol (EtOH) to these systems. Finally, the effect of temperature on the metal-induced hyperchromicity was studied in the temperature range ca. 5 – 20 ^oC below the melting temperature of the respective duplexes. All duplex RNAs contained a common, central r(GG) sequence, either with opposing complementary sequence r(CC) or facing a one base r(UAU) loop, thus allowing for evaluation of the influence of local complementarity on reactivity. Knowledge regarding the inherent reactivity of these commonly found RNA-motifs[8] is an important prerequisite for identification of preferred drug target sites in complex RNA sequence contexts, and constitutes an important mile-stone towards development of sequence specific RNA binders. [9]

Experimental

Chemicals and solutions

HPLC grade quality oligonucleotides (5´-CUU CUU GGU UCU CUU-3´ and 5´-AAG AGA ACC AAG AAG-3´ (RNA-1-1), 5´-UU CUU GGU UCU CU-3´ and 5´-AG AGA ACC AAG AA-3´ (RNA-1-1-S), 5´-CUU CUU GGU UCU CUU-3´ and 5´-AAG AGA AUA UAA GAA G-3´ (RNA-1-3), and 5´-CUU CUU CUU G GU UCU CUU CU-3´ and 5´-AG AAG AGA AUAU AAG AAG AAG-3´ (RNA-1-3-X)) were purchased from IBA GmbH (IBA Nucleic Acids Synthesis, Göttingen, Germany). Cisplatin (*cis*-$Pt(NH_3)_2Cl_2$), **1**) and dimethylformamide (DMF) were obtained from Sigma-Aldrich. Sodium dihydrogen phosphate monohydrate ($NaH_2PO_4 \cdot H_2O$), disodium hydrogen phosphate dihydrate ($Na_2HPO_4 \cdot 2\ H_2O$), sodium perchlorate monohydrate ($NaClO_4 \cdot H_2O$), potassium nitate (KNO_3) and silver nitrate ($AgNO_3$) were obtained from Merck. Potassium dihydrogen phosphate (KH_2PO_4) and dipotassium hydrogen phosphate trihydrate ($K_2HPO_4 \cdot 3\ H_2O$) were obtained from Sigma. Ethanol, 95%, was obtained from Solveco. Phosphate buffers were prepared according to literature procedures.[10] A 200 mM NaH_2PO_4/Na_2HPO_4 buffer at pH 5.8 (NaP_i) was prepared by mixing 23 ml of 200 mM NaH_2PO_4 with 2 ml of 200 mM Na_2HPO_4, after which pH was double-checked using a combination electrode. A potassium buffer at pH 5.8 (KP_i) was prepared analogously by mixing 23 ml of KH_2PO_4 with 2 ml of K_2HPO_4. For preparation of 5× stock solution of the working buffers, the previously prepared 200 mM NaP_i or KP_i buffers were diluted to 100 mM NaP_i/KP_i, using equal volumes of 1.0 M $NaClO_4$ or KNO_3 solutions, respectively. Hence, the working buffers contain C_{Na+} = 122 mM and $[PO_4]_{tot}$ = 20 mM (Buffer A) or C_{K+} = 122 mM and $[PO_4]_{tot}$ = 20 mM (Buffer B). A reduced sodium-salt containing buffer (Buffer C; C_{Na+} = 50 mM, $[PO_4]_{tot}$ = 46 mM) was prepared by dilution of the 200 mM NaP_i buffer stock with water. The buffer with 10% ethanol (v/v) (Buffer D; C_{Na+} = 50 mM, $[PO_4]_{tot}$ = 46 mM, 10% EtOH) was prepared by dilution of the 200 mM NaP_i buffer stock with water. RNA, water and buffer stock were mixed, and the samples were annealed. After the annealing, a volume corresponding to 10% (v/v) of ethanol was added, prior to the kinetic run.

Preparation of mono-aquated cisplatin (1a)

A stock solution of **1** was prepared by addition of 3.5 mg of **1** to 1.17 ml DMF. The solution was vortexed (1400 rpm) over night at room temperature to allow for dissolution. A solution of $AgNO_3$ was prepared by dissolving 2.9 mg $AgNO_3$ in 1.74 ml DMF. Dissolution was obtained after vortexing (2200 rpm) during 5 min at room temperature. Aquated cisplatin (*cis*-$[Pt(NH_3)_2Cl(OH_2)]^+$, **1a**) was prepared according to published procedures[11] by addition of 0.98 mole equivalents of $AgNO_3$ in DMF to a solution of **1** in DMF which resulted in precipitation of AgCl(s) and formation of *cis*- and $[Pt(NH_3)_2Cl(DMF)]^+$, the latter which upon dissolution in H_2O is rapidly converted to mono-aquated cisplatin (*cis*-$[Pt(NH_3)_2Cl(OH_2)]^+$, **1a**). The mixture was incubated at 37 °C during shaking (170 rpm) for 24 h in the dark. Precipitated AgCl(s) was removed by two consecutive centrifugations (duration: 3 and 2.5 h). The supernatant was transferred to new Eppendorf tubes after each centrifugation step. Stock solutions of **1a** were stored in a desiccator together with silica gel, and were kept in the dark at room temperature.

Thermal melting studies

Thermal melting studies were performed on a Varian Cary 4000 spectrophotometer, equipped with a thermal control unit. Hybridized duplex RNAs of RNA-1-1, RNA-1-1-S, RNA-1-3 and RNA-1-3-X were obtained by combination of equal concentrations of (a)- and (b) strands (typically $C_a = C_b = C_{dsRNA}$ 1.5 µM, *i.e.* C_T = 3.0 µM) in buffered solution (Buffers A, B, C and D). The mixture was first heated to 90 °C and then allowed to hybridize by slow cooling (0.5 °C/min) to 20 °C. The samples were held at 20 °C for 5 min, and the melting curve was then collected during heating (0.50 °C/min) to 90 °C. The thermal melting points (T_m) were evaluated by the first derivative method, using the Cary WinUV software. Data points were collected every 0.20 °C, and the equidistant data was used for the Savitzky-Golay calculations.[12] Theoretical estimates of T_m-values at C_{Na+} = 1.0 M were made using the DINAMelt Web Server.[13]

Kinetic studies

Prior to initiation of kinetic experiments, the complementary oligonucleotides were annealed by heating to 90 °C, followed by hybridization by slow cooling (0.5 °C/min) to 20 °C as described above. The duplexes were then heated to 38 °C (0.5 °C/min), and were incubated at this temperature for 5 min, after which **1a** was added, giving final concentrations of $C_{\mathbf{1a}}$ = 7.5, 15.0, 22.5, 30.0 and 45.0 µM. The kinetics of the reaction between **1a** and the RNA duplexes were followed by measuring the change in absorbance at λ = 260 nm for up to ca. 19 h. Experiments were repeated in triplicates for each platinum concentration employed when nothing else stated. The effect of decreasing polarity of the solvent on kinetics was studied with $C_{\mathbf{1a}}$ = 15 µM and C_T = 3.0 µM in a Buffers C and D, *i.e.* with and without 10% (v/v) ethanol, the latter added after the annealing step. Kinetics were performed as described earlier, with $C_{\mathbf{1a}}$ = 15 µM. The temperature dependences of the platination reaction were studied in Buffer A. RNA duplexes were annealed as described earlier, and were then heated from 20 °C (0.5 °C/min) to the studied temperatures, after which **1a** was added; $C_{\mathbf{1a}}$ = 15 µM and C_T = 3.0 µM. The kinetics were studied at four different temperatures, 5.0 °C apart, all below the melting temperature (T_m) of the respective duplexes. The range was from 33.0 °C to 48.0 °C for both RNA-1-1-S and RNA-1-3-X, from 23.0 °C to 38.0 °C for RNA-1-3 and from 33.0 °C to 58.0 °C for RNA-1-1.

Enthalpies and entropies of activation were determined by a fit of the Eyring equation to the natural logarithm of the apparent second-order rate constants divided by the absolute temperature ($k_{2,app}/T$) as a function of 1/*T*, Eq. (1), where $\Delta H^{\neq}$ and $\Delta S^{\neq}$ denote the activation enthalpy and –entropy, respectively, *R* the gas constant, k_B the Bolzmann constant, and *h* refers to Planck´s constant.

$$\ln\left(\frac{k_{2,app}}{T}\right) = \ln\frac{k_B}{h} + \frac{\Delta S^{\neq}}{R} - \left(\frac{\Delta H^{\neq}}{R}\right)\cdot\left(\frac{1}{T}\right) \qquad (1)$$

Structure modelling

Three dimensional (3D) structures of both duplex types, *i.e.* with central full complementarity and bulge respectively, were modelled using the RNA Denovo protocol at the online server ROSIE, Rosetta Online Server That Includes Everyone,[14] using RNA-1-1 and RNA-1-3 as representative duplexes. The updated (2012) force field was used, 1000 structures were generated using 10000 Monte Carlo cycles, and bulges were allowed for. Bond lengths and angles were not varied. The calculations were checked for convergence by plotting the Rosetta all-atom score *vs* rmsd to best scoring model (**Figures S1A** and **S1B**, for RNA-1-1 and RNA-1-3, respectively). The top ranked cluster center models were used and the structures were visualised using PyMOL.[15]

Results

Sequence design and melting temperature

In this work, thermodynamic and kinetic studies have been conducted with the aim to investigate the influence of target size and solvent conditions on the reactivity of the highly nucleophilic r(GG) sequence towards the active metabolite of cisplatin (**1a**). Two closely related RNA duplexes were chosen to allow for facile comparison, also with previously reported data; either with the centrally located r(GG) opposing r(CC) (RNA-1-1 and RNA-1-1-S), or the centrally located r(GG) opposing r(UAU) (RNA-1-3 and RNA-1-3-X). These RNAs share thermodynamic properties with many short-size non-coding RNAs, despite their somewhat truncated size 13 – 20 mer duplexes.[8d, 8f]

Melting temperatures (T_ms) were obtained by analysis of the absorbance change as a function of increasing temperature after annealing. Four different solvent conditions were employed with *i*) extracellularly relevant Na^+-concentration (C_{Na+} = 122 mM, Buffer A), *ii*) intracellularly relevant K^+-concentration (C_{K+} = 122 mM, Buffer B), and *iii*) in a medium containing 10% EtOH and C_{Na+} = 50 mM (Buffer D) with a compative study with C_{Na+} = 50 mM but no EtOH (Buffer C). The data is summarized in **Table 1** (spectra and melting curves in **Figures S2A** and **S2B**) As shown in the table, the melting temperatures of the studied 13- to 20-mer RNA duplexes range from ca. 36 to 62 °C at $C_{Na+/K+}$ = 122 mM, and exhibit the same order of T_ms in the presence of both Na^+ and K^+. Introduction of the central mismatches has a pronounced effect on duplex stability. More precisely, the centrally destabilized 13- and 20-mers RNA-1-3 and -1-3-X (T_m ca. 39 and 53 °C with C_{Na+} = 122 mM, respectively) have T_ms that are ca. 10 – 30 °C lower compared with the fully complementary 13- and 15-mers RNA-1-1-S and -1-1 (T_m ca. 57 and 62 °C with C_{Na+} = 122 mM, respectively). Also, a common tendency of decreased stability

by ca. 2 – 3 °C is observed after replacement of Na^+ for K^+ in the medium. For example, the T_m decreases from ca. 39 to 36 °C for the least stable duplex RNA-1-3, and from ca. 62 °C to 59 °C for the most stable duplex RNA-1-1. Further, reduction of the salt concentration to C_{Na+} = 50 mM results in significant destabilization of these duplexes by ca. 6 – 7 °C (ΔT_m = -6.7, -6.9, -5.8, -6.7 °C for RNA-1-1, -1-1-S, -1-3-X, and -1-3, respectively), with maintained order of T_ms. In contrast, introduction of EtOH has a small non-systematic effect on T_ms. For example, the largest decrease of T_m is obtained for RNA-1-1-S (ΔT_m = -3.1 °C), whereas a non-significant increase is observed for RNA-1-3 (ΔT_m = 0.5 °C) when data at C_{Na+} = 50 mM is compared. Taken together, we conclude that reduction of salt concentration from C_{Na+} = 122 to 50 mM leads to significant reduction of T_ms for all duplex RNAs. In contrast, the influence on T_m caused by a change from Na^+ to K^+ is rather small (2-3 °C) but with a common trend towards destabilization, whereas introduction of EtOH causes only a marginal effect, however also with a tendency towards destabilization.

Metal induced hyperchromicity and half-lives

Platination of duplex nucleic acid structures with cisplatin and related compounds typically results in structural distortion, and with a decrease of T_m as a result.[16] For RNA duplexes investigated close to their respective T_ms, this metal induced lowering of T_m, and concomitant hyperchromicity of the system around λ = 260 nm, has recently been shown by us to be useful for monitoring reactivity by UV/vis spectroscopy.[3l-n] A typical example of spectral changes occurring as a function of time after addition of **1a** to RNA-1-3-X is shown in **Figure 1A**. As illustrated here, the hyperchromicity is accompanied by the expected bathochromic shift,[17] here of ca. 2 nm; from ca. 258 nm to 260. Examples of the change in absorbance as a function of time following addition of excess **1a** to duplex RNAs are shown in **Figures 1B** (RNA-1-1, RNA-1-1-S and RNA-1-3-X, all at 38 °C) and **1C** (RNA-1-3 at 28 °C). As can be seen here, the absorbance changes at λ = 260 nm (ΔA_{260}) are all well described by single-exponential functions. Further, the largest ΔA-value is observed for RNA-1-3-X, followed by RNA-1-1 and then RNA-1-1-S. These ΔA_{260} correspond to a hyperchromicity of ca. 16 – 20% for each dsRNA, and thus indicative of substantial melting and/or degree of dissociation of the duplex following addition of **1a**. Finally, the obtained kinetic traces reveal significantly different reactivity for each of these sequences with half-lives ($t_{1/2}$) in the hour-range. For example, RNA-1-1-S reacts with $t_{1/2}$ ca. 42 min at 38 °C whereas RNA-1-1 has $t_{1/2}$ ca. 56 min under the same reaction conditions with $C_{\mathbf{1a}}$ = 15 μM, compare **Figure 1B**. The order of reactivity correlates with T_ms, and shows increasing reactivity as a function of decreasing T_m with $k_{2,app}$ according to: RNA-1-1 < RNA-1-1-S < RNA-1-3-X < RNA-1-3, see **Table 1** and below for more detailed discussion.

Metal induced kinetics

Reactivity at biologically relevant salt concentrations

Small size duplex RNAs are crucial components of both intra- and extra cellular environments.[4, 18] Thus, with a reactivity similar to that of DNA, scavenging of platinum based drugs is likely to occur in both environments. In order to gain further insights into reactivity in these two environments, reaction conditions mimicking the extracellular (C_{Na+} ca. 0.1 M) and intracellular conditions (C_{K+} ca. 0.1 M) were next employed[19] and compared.

The concentration dependence was determined using excess concentration of **1a**, and treatment of the data according to pseudo-first-order conditions. The studies were conducted at 38 °C for RNA-1-1, RNA-1-1-S and RNA-1-3-X, and at 28 °C RNA-1-3, thus allowing for these RNAs to be present in predominantly duplex state (compare **Figure S1B**). Representative kinetic traces at varying $C_{\mathbf{1a}}$ are shown for the reaction of RNA-1-3-X in K^+-buffer (Buffer B) in **Figures 2A** and **2B** (complete dataset in **Figure S3**) together with fits of single-exponential functions. As illustrated here, the time-dependences are well described assuming pseudo-first-order kinetics with apparent half-lives in the 20 min – 1 h range, and resulting pseudo-first-order rate constants in the range ca. (3 – 10) $\times 10^{-4}$ s^{-1} at the highest platinum concentration employed ($C_{\mathbf{1a}}$ = 45 μM), compare **Table S1**. Further, the pseudo-first-order rate constants exhibit linear dependence on the concentration of **1a**, thus allowing for determination of the apparent second-order rate constant for the reaction ($k_{2,app}$) directly from the slope of a plot of k_{obs} *vs* $C_{\mathbf{1a}}$, compare **Figure 2C**. The obtained values of $k_{2,app}$ are summarized in **Table 1**. As illustrated by the example with RNA-1-3-X in **Figure 2C**, the reactivity in the K^+-environment was significantly above that in the Na^+-environment, despite the rather small change of T_ms between these two buffers, *vide supra*. In summary, a common reactivity trend was observed with increasing reactivity following a decrease of T_m, when the latter was caused by the change from Na^+-buffer to K^+-buffer. For example, the second-order rate constant obtained for the high melting 15-mer RNA-1-1 increased from ca. 7.7 to 9.2 $M^{-1}s^{-1}$ following a change from Na^+- (T_m = ca. 61 °C) to K^+-buffer (T_m ca 59.5 °C). Similarly, for the low melting 20-mer RNA-1-3-X the second-order rate constant increased from ca. 16 to 19 $M^{-1}s^{-1}$ following the same change from Na^+-buffer (T_m = 53 °C) to K^+-buffer (T_m = 51 °C). In contrast, reactivity was found to be uncorrelated with overall dsRNA size, with the intermediate size 15-mers RNA-1-1 and RNA-1-3 exhibiting both highest and lowest extremes with respect to T_ms and $k_{2,app}$.

Influence of hydrophobic solvents on reactivity; 10% EtOH

RNA *in vivo* is often found associated with proteins.[20] By such aggregation, the solvent accessibility of the RNA surface is significantly reduced, for example by creation of local environments with hydrophobic character. To further improve our understanding of how the creation of such environments affect RNA reactivity, a study was next performed in the presence of 10% EtOH (Buffer C). The fraction of EtOH

employed was chosen in agreement with earlier model system studies illustrating the influence of increased hydrophobicity on structure and reactivity.[21] To allow for good kinetic discrimination between experiments, a salt concentration of C_{Na+} = 50 mM was chosen, and two different temperatures were employed, either 38 °C or 28 °C, the latter used for monitoring of the low-melting RNA-1-3. Observed pseudo-first-order and apparent second-order rate constants are summarized in **Table S2** and were obtained by the relationship $k_{2,app} = k_{obs}/C_{\mathbf{1a}}$ (discussed further below). Both the decrease of salt concentration and introduction of EtOH was found to influence reactivity. In the former case, a common ca. 2- to 3-fold increase in reactivity was observed following a decrease from C_{Na+}= 122 to 50 mM, compare **Table 1**. The effect of EtOH was the opposite however, leading to a ca. 30 - 40% reduction of the reactivity for all duplexes studied. This observation thus suggests that the increased reactivity that can be expected to result from *e.g.* local reduction of ionic strength in subcellular compartments is likely compensated for by increased hydrophobicity.

Temperature dependence

The presently employed method for monitoring duplex RNA reactivity relies on the ability of the formed metal adduct(s) to induce RNA hyperchromicity. Further, the amplitude and sensitivity of the method depends on the fraction of converted duplex RNA. The latter is a process that – in analogy with melting of native duplex DNAs – exhibits strong temperature dependence, and particularly so in the region around and below the melting point. So far, we have been able to show that our methodology can be used to monitor reactivity for temperatures just below the T_m, where the proportion of duplex material dominates, see **Figure 3A** (complete dataset in **Figure S4**). To better understand the effect of temperature on the reactivity, a systematic temperature dependence study was therefore next performed. The reactions were studied in the temperature range where duplex RNA predominates, but the equilibrium between duplex- and single-stranded RNA is sensitive towards small temperature variations, *i.e.* in the range down to ca. 20 °C below T_m. As illustrated by the example with RNA-1-1-S in **Figure 3**, a significant temperature dependence of the reaction rate was found in this temperature region. Typically, the reduction in reactivity was found to be 4– to 7- fold following a 10 °C decrease of temperature (**Table S3**).

To further characterize the temperature dependence, the apparent second-order rate constants were subjected to analysis by the Eyring equation (**Eq. 1**). With the type of reaction studied here, *i.e.* a pre-equilibrium followed by a rate determining step (discussed further below) the obtained apparent activation parameters $\Delta H^{\neq}_{app}$ and $\Delta S^{\neq}_{app}$ correspond to the sum of contributions from these two steps,[22] and thus likely reflect the process of combined *i*) association and coordination of **1a** to the RNA and *ii*) duplex dissociation. An inspection of the data summarized in **Table 2** reveals positive values of both $\Delta H^{\neq}_{app}$ (ca. 23 – 34 kcal mol^{-1}) and $\Delta S^{\neq}_{app}$ (ca. 22 – 57 cal K^{-1} mol^{-1}), with the upper limits represented by the data for the 20-mer RNA-1-3-X and lower ones for the 15-mer RNA-1-1-S. These data suggest that the increase of $\Delta H^{\neq}_{app}$ caused by increased global duplex stability of the RNA-1-3-X is partially compensated for by an increase also in $\Delta S^{\neq}_{app}$. It should be noted that this is a phenomenon typically observed for melting of duplex nucleic acids alone, where an increase of duplex size is intimately associated with increased release of surface bound both solvent- and counter-ions during melting.[23]

Structure modelling

In contrast to DNA, the task of obtaining experimentally determined solid state structures for RNA is still challenging,[24] and data of relevance for our here investigated systems seem still to be lacking. To gain insights into tentative structures of the currently used RNA targets, structural modelling was therefore conducted using RNA-1-1 and RNA-1-3 as representative sequences. For the complementary RNA-1-1, the structure converged towards a symmetric helical structure, and with parameters in close agreement with expectations based on standard A-RNA formation, see **Figure 4**. In contrast, introduction of the central bulge r(UGGU)·r(AUAUA) in RNA-1-3 results in a bend and kink of the structure. More precisely, the central A mismatch is able to compete with neighboring U-bases for base-pairing with the opposing Gs (**Figure 4B**, right). This base-pairing ambivalence leads to substantial distortion of both H-bonding and stacking interactions in the central region of the duplex compared with the A-type arrangement found for RNA-1-1 (**Figure 4A**, right).

Discussion

Mechanism and activation parameters

A large portion of the intravenously injected cisplatin interacts directly with components of the blood system.[25] Further, a major part of distributed cisplatin is excreted within the first hours of administration.[26] Nevertheless, the small portion that reaches its target cell is transported over the cellular membrane, most likely as a combination of passive and active transport.[1d, 27] Inside the cell, the low chloride ion concentration allows for hydrolysis of the parent compound to take place, and formation of charged and more reactive metabolites, *e.g. cis*-$[Pt(NH_3)_2Cl(OH_2)]^+$ (**1a**) is thermodynamically favoured.[1c, 1d, 27a] As a charged species, **1a** is attracted to the polyanionic surfaces of nucleic acids, where it likely acts as a temporary counterion prior to the rate-determining formation of the covalent adduct.[27b, 28] For small size RNAs, it seems likely that formation of the adduct takes place during substantial reorganisation of duplex structures during partial or complete melting of the dsRNA.[3l-n] A tentative simplistic reaction mechanism for our here investigated systems is outlined in Eqns (2) - (4), and the corresponding rate-law is given in Eqns (5a) and (5b).

1a + dsRNA···M^+ ⇄ **1a** ··· dsRNA + M^+ K_{ass} (2)

1a ··· dsRNA → **1a** — dsRNA k (3)

1a — dsRNA → **1a** — ssRNA(a) + ssRNA(b) *rapid* (4)

$$k_{obs} = k_{2app}[\mathbf{1a}][\text{dsRNA}\cdots M^+] \quad (5a)$$

$$\text{where } k_{2app} = k\,K_{ass}/[M^+] \quad (5b)$$

The mechanism implies that the salt dependent variation of $k_{2,app}$ arises from displacement of the equilibrium in Eq. (2) where one surface bound monovalent cation, *e.g.* Na^+, is replaced by surface bound **1a**, compare also Eq. (5b). Under these assumptions, the product kK_{ass} for each dsRNA can be obtained by the relation $kK_{ass} = k_{2,app}$ $[M^+]$. In agreement with this prediction, constant values of kK_{ass} are indeed obtained for each dsRNA with values ranging from ca. 1 for RNA-1-1 to 3.62 for RNA-1-3 (compare **Table S4**). By assuming an approximate value of K_{ass} ca. 1,[29] leads to an estimation of the conversion of surface bound **1a** to covalent adduct of about 1 – 2 s^{-1}, and a corresponding $t_{1/2}$ for the surface bound **1a** of ca. 0.3 – 0.7 s.

Sequence and structural influence on reactivity

In DNA, guanine-N7 (G-N7) is a well documented preferential interaction site for cisplatin. The precise location is sequence dependent however; typically with d(GpG) and d(ApG) as the two dominating adduct sites in extended DNA.[30] The underlying reason for this selectivity has been ascribed to a combination of kinetic and thermodynamic effects, where factors such as hydrogen bonding networks in the close vicinity of the adduct, combined with favourable dynamics of the duplex, dictates reactivity.[7] For the structurally diverse family of RNAs, the issue regarding sequence dependent reactivity has not – to the best of our knowledge – been systematically studied. The structural models provided in the present investigation give however a first insight into how subtle variations of sequence and solvent conditions may modulate the reactivity of the r(GpG)-site. As illustrated in **Figure 4**, introduction of the bulge in RNA-1-3 causes the RNA to both bend and widen when compared to RNA-1-1. Further, the schematic illustrations of H-bonding patterns in the central region of these duplexes (**Figure 4**, right) show that this distortion likely involves a structure in which the central r(A)-base competes with one of the two proximal GU-wobble bases for hydrogen bonding, thus giving a rationale for the pronounced decrease of T_m and high reactivity for this type of structure,[3n] compared with the corresponding RNA duplex lacking a central r(A). It seems possible that these structural differences influence reactivity, for example by their different ability to temporarily host bulk cations in the vicininty of the taget site. More precisely, the more pronounced electronegativity and smaller radius of Na^+ (0.93 and 95 pm, respectively) compared to K^+ (0.82 and 133 pm) likely contributes to both more tightly bound cations and rigid structure compared to in the presence of K^+. Both these effects will make surface access for **1a** to G-N7 more difficult in the presence of Na^+, since the mobility of both solvent water molecules and cations is reduced,[31] and can thus explain the here observed lower reactivity in Na^+-containing buffer. It should be noted that the study by Nordenskiöld et al.[31] also showed that the residence locations for these two cations differ; Na^+ has a preference for phosphate oxygen interactions whereas K^+ has a more pronounced residency time at the nucleobases. This is an effect that in our system should counteract the influence from solvent exchange on the surface discussed above. We therefore conclude that the rate of solvent exchange more strongly influences reactivity in our presently investigated systems than does actual location of these counterions.

Temperature dependence and activation parameters

The reaction mechanisms for substitution reactions involving cisplatin and its corresponding aquated complexes typically proceed via an associative interchange mechanism (I_a).[17, 32 33] For this mechanism the reaction rate depends on the concentration of both the metal complex and the approaching nucleophile. Further, analysis of the temperature dependence result in activation enthalpies ($\Delta H^{\neq}$) that are dominated by the energy required for formation of the penta-coordinated transition state, *i.e.* with leaving- and entering ligands coordinated, and with a negative activation entropy ($\Delta S^{\neq}$) that reflects the concomitant loss of entropy in the system. For example, Summa and van Eldik[33] have documented reactions of $Pt(dach)(OH_2)_2^{2+}$ and $Pt(en)(OH_2)_2^{2+}$ with 5′-GMP resulting in activation parameter of $\Delta H^{\neq}$ ca. 14 – 17 $kcalmol^{-1}$ and $\Delta S^{\neq}$ ca. -2 – -7 $kcalK^{-1}mol^{-1}$. In the present study we now present temperature dependent data that allows for a comparison between these small model systems and reactions taking place on extended dsRNA. As shown in **Table 2**, the $\Delta H^{\neq}$ -values obtained are ca. 23 – 34 $kcalmol^{-1}$, *i.e.* significantly larger compared with the model system studies mentioned above using 5′-GMP as a nucleophile.[33] Further, the $\Delta S^{\neq}$ -values obtained are all positive, here in the range 22 – 57 $kcalK^{-1}mol^{-1}$. With the type of mechanism outlined in Eqns. (2) – (4) it is obvious that the activation parameters reflect the combined contributions from *i*) the pre-equilibrium (Eq. 2) and *ii*) the formation of the covalent adduct (Eq. 3).[22] Since the rapid pre-equilibrium likely has a very small activation barrier,[29, 34] we propose that the larger portion of $\Delta H^{\neq}$ arises from the energy required for adduct formation and related local disruption of duplex structure (Eq. 3). More specifically, we suggest that the larger $\Delta H^{\neq}$-values obtained for the dsRNA reactions are associated with the additional energy needed for breaking of both stacking- and H-bonding interactions in the vicinity of the binding site during formation of the penta-coordinated transition state. We thus propose that this initial interaction creates a centrally destabilized dsRNA that, at temperatures close to the T_m of the unplatinated dsRNA, in a subsequent rapid step dissociates into single-stranded RNAs (Eq. (4)), *i.e.* in analogy with previous suggestions made for DNA.[17] The positive $\Delta S^{\neq}$-values are in support of such reaction mechanism since these imply that the reaction occurs during net loss of hydration and/or counterions from the RNA surface. It should

be noted that the activation energies are significantly smaller in magnitude in comparison to global melting of dsRNAs, (compare **Table 3**) thus further supporting of the idea of partial melting of the dsRNA as the initial process accompanying adduct formation.

Conclusions

In the present study, we have compared the reactivity of four closely related dsRNAs towards the active metabolite of cisplatin (*cis*-$[Pt(NH_3)_2Cl(OH_2)]^+$, **1a**). For these 13-20 mer dsRNAs, all with a centrally located r(GG) site, similar reactivity orders were obtained in presence of both extra- and intracellularly relevant cation concentrations (K^+ and Na^+, respectively) as well as under more hydrophobic conditions (10% v/v EtOH). A common trend of central destabiliziation, and related reduction of T_m, rather than overall size, was found to promote reactivity. A comparison of apparent second-order rate constants ($k_{2,app}$) reveals the reactivity to be slightly higher in K^+-containing buffer compared to that obtained with Na^+, thus indicative of the intracellular environment being favoured compared to the extracellular one for reactions of **1a** with dsRNAs. The presence of EtOH in the buffer resulted in a reduction of $k_{2,app}$ with ca. 30 – 40% for all dsRNAs studied, *i.e.* suggesting that association of dsRNAs in hydrophobic comparments *in vivo* decreases their reactivity substantially. Apparent activiation paraments were obtained by studies of the reactivity as a function of temperature in the range ca. 5 – 20 ^oC below the T_m of all dsRNAs. The extracted parameters were similar for all systems with positive both $\Delta H^{\neq}$ and $\Delta S^{\neq}$. The positive $\Delta S^{\neq}$-values are indicative of the rate-determinig step occurring in parallel with partial loss of hydration and/or cations, for example during partial melting of the dsRNA structure in the vicinity of the common central binding site r(GG). These observations thus support the idea of local melting behaviour and dynamics to be a major determinant for adduct formation rates in dsRNAs.

Acknowledgements

Financial support from Cancerfonden (Grant No. 13 0317), Kungl. Fysiografiska Sällskapet i Lund, Crafoordska stiftelsen, and FLÄK (Reseach School in Pharmaceutical Science at Lund U) and COST action CM1105 is gratefully acknowledged.

Notes and references

[a] Biochemistry and Structural Biology, KILU, Lund University, POBox 124, SE-221 00 Lund, Sweden. *Corresponding author; E-mail: sofi.elmroth@biochemistry.lu.se

Electronic Supplementary Information (ESI) available: Melting temperatures together with observed rate constants at C_{Na+} = C_{K+} = 122 mM (Table S1), Observed pseudo-first-order rate constants at C_{Na+} = 50 mM with and without 10% EtOH (Table S2), Second-order rate constants as a function of temperature (Table S3), List of obtained products $k_{2,app}C_{Na+}$ (Table S4), Rosetta all-atom score *vs* rmsd (Figure S1), Spectra and melting curves (Figure S2), Primary kinetic data collected in Buffers B, C, and D together with concentration dependence in Buffer B (Figure S3), Temperature dependence and Eyring plots (Figure S4). See DOI: 10.1039/b000000x/

1. a) B. Rosenberg, L. VanCamp, J. E. Trosko and V. H. Mansour, *Nature*, 1969, **222**, 385; b) L. Kelland, *Nat. Rev. Cancer*, 2007, **7**, 573; c) Y. W. Jung and S. J. Lippard, *Chem. Rev.*, 2007, **107**, 1387; d) A. Maccio and C. Madeddu, *Expert Opin. Pharmacother.*, 2013, **14**, 1839.
2. a) A. Mandic, J. Hansson, S. Linder and M. C. Shoshan, *J. Biol. Chem.*, 2003, **278**, 9100; b) F. Yu, J. Megyesi and P. M. Price, *American Journal of Physiology-Renal Physiology*, 2008, **295**, F44; c) S. Dasari and P. B. Tchounwou, *Eur. J. Pharmacol.*, 2014, **740**, 364.
3. a) M. Akaboshi, K. Kawai, H. Maki, K. Akuta, Y. Ujeno and T. Miyahara, *Jpn. J. Cancer Res.*, 1992, **83**, 522; b) T. D. Schmittgen, J. F. Ju, K. D. Danenberg and P. V. Danenberg, *Int. J. Oncol.*, 2003, **23**, 785; c) M. Hägerlöf, P. Papsai, C. S. Chow and S. K. C. Elmroth, *J. Biol. Inorg. Chem.*, 2006, **11**, 974; d) M. Hägerlöf, H. Hedman and S. K. C. Elmroth, *Biochem. Biophys. Res. Commun.*, 2007, **361**, 14; e) P. Papsai, J. Aldag, T. Persson and S. K. C. Elmroth, *J. Chem. Soc., Dalton Trans.*, 2006, 3515; f) P. Papsai, Å. S. Snygg, J. Aldag and S. K. C. Elmroth, *Dalton Trans.*, 2008, 5225; g) K. Rijal and C. S. Chow, *Chem. Commun.*, 2009, 107; h) H. K. Hedman, F. Kirpekar and S. K. C. Elmroth, *J. Am. Chem. Soc.*, 2011, **133**, 11977; i) E. G. Chapman, A. A. Hostetter, M. F. Osborn, A. L. Miller and V. J. DeRose, *Metal Ions in Life Science*, 2011, **9**, 347; j) A. A. Hostetter, M. F. Osborn and V. J. DeRose, *ACS Chem. Biol.*, 2012, **7**, 218; k) G. Hermann, P. Heffeter, T. Falta, W. Berger, S. Hann and G. Koellensperger, *Metallomics*, 2013, **5**, 636; l) C. Polonyi and S. K. C. Elmroth, *Dalton Trans.*, 2013, **42**, 14959; m) C. Polonyi, I. Albertsson, M. S. Damian and S. K. C. Elmroth, *Z. Anorg. Allg. Chem.*, 2013, **639**, 1655; n) C. Polonyi, A. Alshiekh, L. A. Sarsam, M. Clausen and S. K. C. Elmroth, *Dalton Trans.*, 2014, **43**, 11941; o) M. F. Osborn, J. D. White, M. M. Haley and V. J. DeRose, *ACS Chem. Biol.*, 2014, **9**, 2404.
4. B. Gyoergy, M. E. Hung, X. O. Breakefield and J. N. Leonard, *Annual Review of Pharmacology and Toxicology, Vol 55*, 2015, **55**, 439.
5. a) M. Hägerlöf, P. Papsai, H. K. Hedman, U. Jungwirth, V. Jenei and S. K. C. Elmroth, *J. Biol. Inorg. Chem.*, 2008, **13**, 385; b) J. P. Becker, J. Weiss and D. Theile, *Toxicol. Lett.*, 2014, **225**, 43; c) E. G. Chapman and V. J. DeRose, *J. Am. Chem. Soc.*, 2010, **132**, 1946.
6. A. A. Hostetter, E. G. Chapman and V. J. DeRose, *J. Am. Chem. Soc.*, 2009, **131**, 9250.
7. J. Kozelka, *Inorg. Chim. Acta*, 2009, **362**, 651.
8. a) D. A. Peattie, S. Douthwaite, R. A. Garrett and H. F. Noller, *P. Natl. Acad. Sci. USA-Biol.*, 1981, **78**, 7331; b) S. Althoff, D. Selinger and J. A. Wise, *Nucleic Acids Res.*, 1994, **22**, 1933; c) R. R. Gutell, J. J. Cannone, Z. Shang, Y. Du and M. J. Serra, *J. Mol. Biol.*, 2000, **304**, 335; d) S. Griffiths-Jones, *Nucleic Acids Res.*, 2004, **32**, D109; e) P. Dua, J. W. Yoo, S. Kim and D. K. Lee, *Mol. Ther.*, 2011, **19**, 1676; f) A. Kozomara and S. Griffiths-Jones, *Nucleic Acids Res.*, 2011, **39**, D152.
9. a) L. Guan and M. D. Disney, *ACS Chem. Biol.*, 2012, **7**, 73; b) S. P. Velagapudi, S. M. Gallo and M. D. Disney, *Nat. Chem. Biol.*, 2014, **10**, 291; c) V. Duc Duy, C. Staedel, L. Zehnacker, R. Benhida, F. Darfeuille and M. Duca, *ACS Chem. Biol.*, 2014, **9**, 711; d) A. Mehta, S. Sonam, I. Gouri, S. Loharch, D. K. Sharma and R. Parkesh, *Nucleic Acids Res.*, 2014, **42**, D132; e) M. D. Disney, *Drug Discov. Today*, 2013, **18**, 1228; f) S. Bellaousov, J. S. Reuter, M. G. Seetin and D. H. Mathews, *Nucleic Acids Res.*, 2013, **41**, W471.
10. D. D. Moore, *Curr. Protoc. Mol. Biol.*, 2001, **35**, A.2.1.
11. W. I. Sundquist, D. P. Bancroft and S. J. Lippard, *J. Am. Chem. Soc.*, 1990, **112**, 1590.
12. A. Savitzky and M. J. E. Golay, *Anal. Chem.*, 1964, **36**, 1627.

13. a) N. R. Markham and M. Zuker, *Nucleic Acids Res.*, 2005, **33**, W577; b) N. R. Markham and M. Zuker, *Methods in Molecular Biology:VOLUME II: STRUCTURE, FUNCTION AND APPLICATIONS*, 2008, **453**, 3.
14. a) R. Das, J. Karanicolas and D. Baker, *Nat. Methods*, 2010, **7**, 291; b) S. Lyskov, F.-C. Chou, S. O. Conchuir, B. S. Der, K. Drew, D. Kuroda, J. Xu, B. D. Weitzner, P. D. Renfrew, P. Sripakdeevong, B. Borgo, J. J. Havranek, B. Kuhlman, T. Kortemme, R. Bonneau, J. J. Gray and R. Das, *PLOS One*, 2013, **8**.
15. *The PyMOL Molecular Graphics System, Version 1.6.0.0 Schrödinger, LLC.*, http://www.pymol.org/citing.
16. a) P. M. Takahara, A. C. Rosenzweig, C. A. Frederick and S. J. Lippard, *Nature*, 1995, **377**, 649; b) B. Spingler, D. A. Whittington and S. J. Lippard, *Inorg. Chem.*, 2001, **40**, 5596; c) H. C. Harder, *Chem.-Biol. Interact.*, 1975, **10**, 27; d) J. P. Macquet and J. L. Butour, *Biochimie*, 1978, **60**, 901; e) S. E. Sherman and S. J. Lippard, *Chem. Rev.*, 1987, **87**, 1153.
17. P. Horacek and J. Drobnik, *Biochim. Biophys. Acta*, 1971, **254**, 341.
18. a) M. S. Rodriguez, C. Dargemont and F. Stutz, *Biol. Cell*, 2004, **96**, 639; b) B. H. Zhang, Q. L. Wang and X. P. Pan, *J. Cell. Physiol.*, 2007, **210**, 279; c) E. E. Creemers, A. J. Tijsen and Y. M. Pinto, *Circ. Res.*, 2012, **110**, 483; d) S. Principe, A. B.-Y. Hui, J. Bruce, A. Sinha, F.-F. Liu and T. Kislinger, *Proteomics*, 2013, **13**, 1608.
19. D. Rehder, *Bioinorganic Chemistry*, Oxford University Press, 2014.
20. B. Rozycki and E. Boura, *J. Phys.-Condens. Mat.*, 2014, **26**.
21. a) D. D. Albergo and D. H. Turner, *Biochemistry*, 1981, **20**, 1413; b) K. M. Guckian, B. A. Schweitzer, R. X. F. Ren, C. J. Sheils, D. C. Tahmassebi and E. T. Kool, *J. Am. Chem. Soc.*, 2000, **122**, 2213; c) M. N. Manalo, X. Kong and A. LiWang, *J. Biomol. NMR*, 2007, **37**, 257.
22. J. H. Espenson, *Chermical Kinetics and Reaction Mechanisms*, McGraw-Hill International Editions, New York, 1995.
23. a) M. Petersheim and D. H. Turner, *Biochemistry*, 1983, **22**, 256; b) S. M. Freier, M. Petersheim, D. R. Hickey and D. H. Turner, *J. Biomol. Struct. Dyn.*, 1984, **1**, 1229; c) A. E. Peritz, R. Kierzek, N. Sugimoto and D. H. Turner, *Biochemistry*, 1991, **30**, 6428; d) T. B. Xia, J. A. McDowell and D. H. Turner, *Biochemistry*, 1997, **36**, 12486.
24. J. Kondo, A.-C. Dock-Bregeon, D. K. Willkomm, R. K. Hartmann and E. Westhof, *Acta Crystallogr. F*, 2013, **69**, 634.
25. A. Casini and J. Reedijk, *Chemical Science*, 2012, **3**, 3135.
26. M. Sathekge, J. Wagener, S. V. Smith, N. Soni, B. Marjanovic-Painter, C. Zinn, C. Van de Wiele, Y. D'Asseler, G. Perkins and J. R. Zeevaart, *Nucl. Med.-Nukl.*, 2013, **52**, 222.
27. a) M. D. Hall, M. Okabe, D.-W. Shen, X.-J. Liang and M. M. Gottesman, *Annu. Rev. Pharmacol.*, 2008, **48**, 495; b) S. K. C. Elmroth and S. J. Lippard, *Inorganic Chemistry*, 1995, **34**, 5234.
28. Å. S. Snygg, M. Brindell, G. Stochel and S. K. C. Elmroth, *Dalton Trans.*, 2005, 1221.
29. N. Korolev, A. P. Lyubartsev, A. Rupprecht and L. Nordenskiöld, *Biophys. J.*, 1999, **77**, 2736.
30. A. M. J. Fichtinger-Schepman, P. H. M. Lohman and J. Reedijk, *Nucleic Acids Res.*, 1982, **10**, 5345.
31. Y. H. Cheng, N. Korolev and L. Nordenskiöld, *Nucleic Acids Res.*, 2006, **34**, 686.
32. J. Arpalahti and B. Lippert, *Inorg. Chem.*, 1990, **29**, 104.
33. N. Summa, W. Schiessl, R. Puchta, N. V. Hommes and R. van Eldik, *Inorg. Chem.*, 2006, **45**, 2948.
34. J. W. Nelson and I. Tinoco, *Biochemistry*, 1982, **21**, 5289.

